

Low-density EEG for Source Activity Reconstruction using Partial Brain Models

Andres Felipe Soler¹, Eduardo Giraldo² and Marta Molinas¹

¹Department of Engineering Cybernetics, Norwegian University of Science and Technology, Trondheim, Norway

²Department of Electrical Engineering, Universidad Tecnológica de Pereira, Pereira, Colombia

Keywords: Low-density EEG, Partial Brain Model, Source Reconstruction, Brain Mapping, EEG Signals.

Abstract: Brain mapping studies have shown that the source reconstruction performs with high accuracy by using high-density EEG montages, however, several EEG devices in the market provide low-density configurations and thus source reconstruction is considered out of the scope of those devices. In this work, our aim is to use a few numbers of electrodes to reconstruct the neural activity using partial brain models, therefore, we presented a pipeline to estimate the brain activity using a low-density EEG on brain regions of interest, the partial brain model formulation and several criteria for channel selection. Two regions have been considered to be studied, the occipital region and motor cortex region. For the presented study synthetic EEG signals were generated simulating the activation of sources with a frequency in the beta range at the occipital region, and mu rhythm range at the motor cortex areas. Novel methods for electrode reduction and models for specific brain areas are presented. We assessed the quality of the reconstructions by measuring the localization error, obtaining a mean localization error below 7 mm and 16 mm with sLORETA and MSP methods respectively, by using a low-density EEG with eight channels and partial brain models.

1 INTRODUCTION

Electroencephalography (EEG) is a non-invasive technique that allows measuring the electrical brain activity from the scalp with a high temporal resolution compared with other techniques like Functional Magnetic Resonance Imaging (fMRI), Computed Tomography (CT), and Positron Emission Tomography (PET). Since the first report about brain activity measured by electrodes was presented by Hans Berger in 1924 (O'Leary, 1970), EEG technique has been used to study various brain processes like memory and emotions, brain diseases like Parkinson and epilepsy, and human behavior, in attempts to understand the complexity underlying processing capabilities of the brain. Source analysis based on brain mapping techniques are allowed to reconstruct the cortical activity from electrodes on the scalp solving the EEG inverse problem. Several methods have been proposed to provide a estimation of the neural activity, like minimum norm estimation MNE (Hämäläinen and Ilmoniemi, 1994) or low-resolution tomography LORETA (Pascual-Marqui et al., 1994).

In brain mapping research, it has been established that a high number of electrodes is required to localize

accurately and reconstruct the cortical activity. However, a few studies have shown the possibility to apply brain mapping methods using a small number of electrodes. E.g, in (Jatoi and Kamel, 2018), the authors proposed and evaluated the use of seven electrodes to map the activity of the whole brain using several brain mapping methods, obtaining a localization accuracy around 15 mm using multiple sparse priors method MSP (Friston et al., 2008). In (Soler et al., 2019), a low-density approach to BCI was presented, in which the occipital activity was mapped using MSP and a partial brain model of the occipital region, obtaining an accuracy around 23 mm in the location of the source with four electrodes using simulated activity, however, a channel selection criteria were not established and the partial brain model was briefly formulated.

The aim of this current study is to establish a pipeline to apply low-density EEG configurations for source activity reconstruction using partial brain models, presenting the formulation to map the brain based on regions of interest. Additionally, several criteria are proposed to perform a selection of the channels to be used for brain mapping, two criteria are considered, one based on local electrodes around the target

zone, and a second one based on a relevance criterion. In this work, we presented a pipeline to estimate the brain activity, to test our methodology, we used synthetic EEG signals, simulating sources over two brain regions, the occipital region, and motor cortex region. We use the localization error to evaluate the reconstructions comparing the position of the estimated sources versus the simulated one.

2 MATERIAL AND METHODS

2.1 Forward EEG Model

The relation between the EEG electrodes distributed on the scalp and the source activity can be represented by the forward problem equation:

$$\mathbf{y} = \mathbf{M}\mathbf{x} + \boldsymbol{\varepsilon} \quad (1)$$

where $\mathbf{M} \in \mathbb{R}^{d \times n}$ represents the volume conductor model, also known by leadfield matrix. This matrix represents the conductivity of the brain and explains how the potentials flow through brain from a set of n distributed sources to d number of electrodes on the scalp. This volume conductor model in realistic brain representations considers the head anatomy and the conductivity of the different tissues and layers between current sources and electrodes, like white matter, gray matter, CSF, skull and scalp (Vorwerk et al., 2012; Huang et al., 2016). $\mathbf{y} \in \mathbb{R}^{d \times k}$ represents the signals recorded by the electrodes in k number of samples, the source activity matrix is represented by $\mathbf{x} \in \mathbb{R}^{n \times k}$, it contains the amplitude of distributed sources over the brain cortical areas. $\boldsymbol{\varepsilon}$ represents the noise covariance, and it is assumed to follow a normal distribution with zero mean.

2.2 Partial Brain Model Formulation

Consider the problem of EEG generation for a time instant given by the forward EEG equation in 1. This model can be rewritten by considering two subsets of brain activity \mathbf{x} as follows:

$$\mathbf{y} = [\mathbf{M}_1 \quad \mathbf{M}_2] [\mathbf{x}_1 \mathbf{x}_2] + \boldsymbol{\varepsilon} \quad (2)$$

being \mathbf{M}_1 and \mathbf{x}_1 being the leadfield matrix and its corresponding neural activity for a specific brain zone of interest or target zone, and \mathbf{M}_2 and \mathbf{x}_2 the leadfield matrix and its corresponding neural activity of the remaining brain. It can be seen that the (2) can be rewritten as

$$\mathbf{y} = \mathbf{M}_1 \mathbf{x}_1 + \boldsymbol{\eta} \quad (3)$$

$\boldsymbol{\eta}$ being a vector that holds the noise and the activity in the part of the brain related to \mathbf{M}_2 and \mathbf{x}_2 . In addition, if the vector \mathbf{x}_2 is close to zero (which means that the neural activity outside the target zone is closed to zero), the following approximation can be performed

$$\mathbf{y} \approx \mathbf{M}_1 \mathbf{x}_1 + \boldsymbol{\varepsilon} \quad (4)$$

By using an approximated model as described in (4) the inverse problem for $\hat{\mathbf{x}}_1$ can be solved. However, the activity outside the target zone could affect the estimation because all the recorded activity by the electrodes will be projected in the target zone. Therefore, an additional stage to reduce the effect of $\mathbf{M}_2 \mathbf{x}_2$ over \mathbf{y} can be added before performing the inverse problem, by considering that the source in the target zone appears in a known frequency, then, the EEG is filtered using band-pass filters leading to an attenuation of the activity outside the region of interest. In addition, by assuming that the electrodes mostly record activity in the neighbor spaces around it, a reduction in the number of electrodes can be made as

$$\mathbf{y}_r \approx \mathbf{M}_{1r} \mathbf{x}_{1r} + \boldsymbol{\varepsilon}_r \quad (5)$$

where the resulting estimation of \mathbf{x}_{1r} is an approximation of \mathbf{x}_1 obtained by using a reduced number of channels.

A partial brain model is a section of the brain based on a specific zone of interest and it is generated from a complete brain model. For that purpose, we used the brain model denominated as the New York Head (ICBM-NY) presented in (Huang et al., 2016), this is based on the computation of a finite element method (FEM) over a non-linear average of 152 individual MRI (ICBM152 v2009) from the International Consortium for Brain Mapping (Fonov et al., 2009). The New York Head was calculated considering the conductivity of six tissue types: scalp, skull, CSF, gray matter, white matter and air cavities with a resolution of $0.5mm^3$. The lead field matrix of the New York Head was calculated for 74382 distributed sources and 231 electrodes, however, several strict subsets of sources with 10016, 5008 and 2004 vertices are available at <https://www.parralab.org/nyhead/>.

We selected the model of 10016 and performed an electrode reduction to 60 positions of the 10-20 international system (Fig.1A), this model is referred to the paper as 10K model and it is used to compare the performance of a high-density montage versus the partial brain models with low-density EEG.

We generated a partial brain model of two brain areas: occipital cortex area (Fig.1B) referred to OC model, and the motor cortex area referred to MC model (Fig.1C). The number of distributed sources for the partial brain models is 3054 for the OC model and 2162 for the MC model.

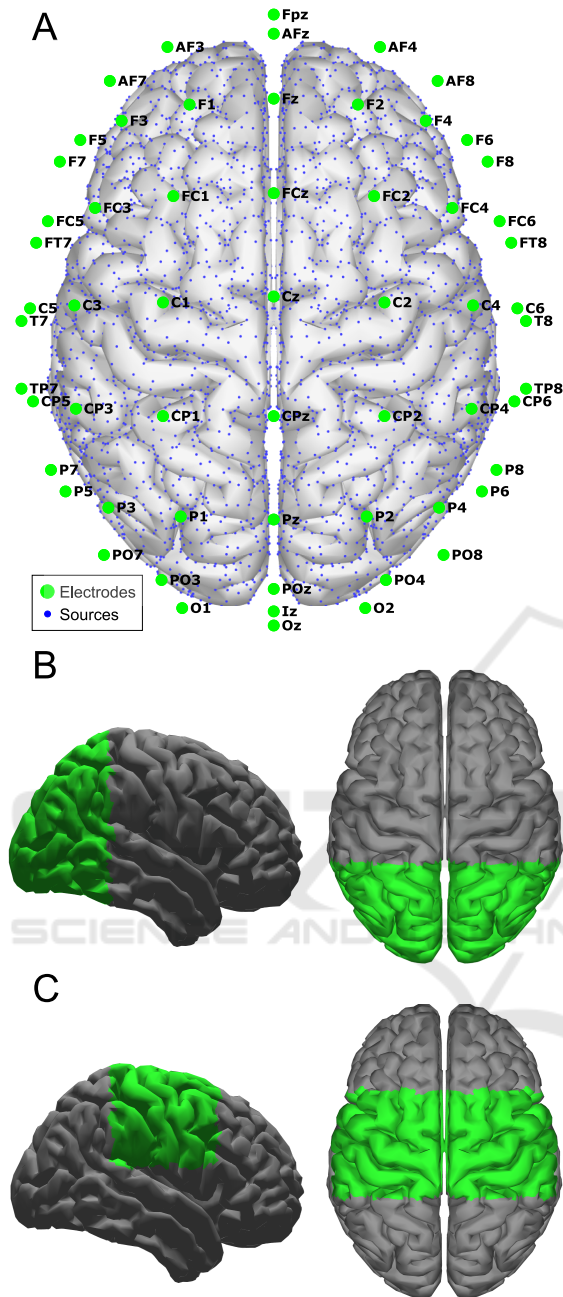


Figure 1: Head model with 60 electrodes and 10016 sources, 10K model (A), Brain section for occipital cortex area partial brain model, OC model (B), and Brain section for motor cortex area partial brain model, MC model (C).

2.3 Synthetic EEG Generation

With the purpose to evaluate the performance of the partial brain models for source reconstruction, we generated 400 trials of simulated EEG activity at five levels of noise: 0, 5, 10, 15, and 20dB (80 trials per level). Each trial has two simulated sources over-

lapping between 37.5% and 40%. Each simulated source activity was computed using a windowed sinusoidal activity using the following equation:

$$x_i(t_k) = e^{-\frac{1}{2}\left(\frac{t_k - c_i}{\sigma}\right)^2} \sin(2\pi f_i t_k) \quad (6)$$

where $\sigma = 0.12$ determines the Gaussian window width. The first source s_1 was simulated in the occipital areas, with a frequency f_1 of 20Hz (simulating a source in the range of Beta wave), and centered at $c_1 = 300ms$. The second source s_2 was simulated in the motor cortex areas, with a frequency f_2 of 10Hz (simulating a source in the range of mu rhythm), and centered at $c_2 = 800ms$. The positions were randomly selected between a set of pre-defined positions distributed on the corresponding target zone. The pre-defined set of positions has six locations, three in each hemisphere, the positions were: 3727, 8735, 2734, 7742, 3461, and 8469 for the source s_1 at occipital areas and 3837, 8845, 2284, 7292, 2271, and 7279 for the source s_2 at motor cortex areas. An example of the simulated activity is shown in Fig.2. It shows the location of the simulated sources at the center of activity and the time courses of the sources during the simulated trial, in addition, the EEG related to the simulated activity is presented with the electrodes labeling.

2.4 Channel Selection

We applied two criteria to select the electrodes: using local electrodes around the region of interest as presented in (Soler et al., 2019), and using a channel relevance analysis applying the Q- α method proposed by (Wolf and Shashua, 2005). Those criteria are explained below:

2.4.1 Local Electrodes

The concept of local electrodes is based on the hypothesis that *the electrodes mostly record the electrical activity of the near space around it*. To select an electrode configuration we considered the results of the previous work of (Soler et al., 2019), in which a four-electrode configuration was used to map one source in the occipital region with a mean localization error of 23 mm. Therefore, to evaluate the concept of local electrodes and compare if increasing the number of electrodes decreases the error, we selected a configuration of eighth electrodes around the target zone, maintaining an equal number of electrodes across both brain hemispheres. Those configurations are shown in Fig.3 for the OC and MC partial brain models.

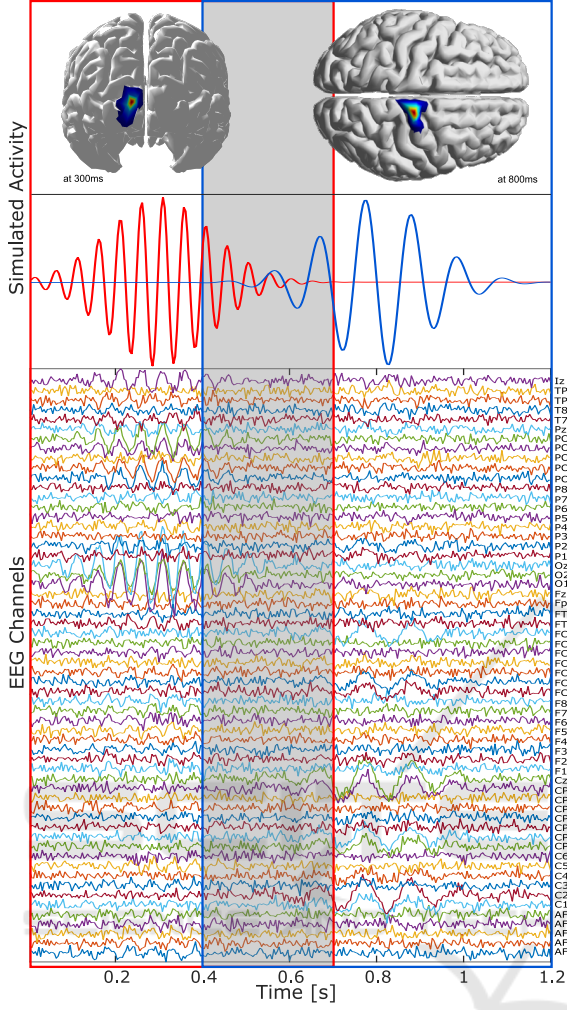


Figure 2: Example of source activity (top), source activity one simulated between 0-0.7s at 20Hz in the occipital area (red), source activity two simulated between 0.4-1.2s at 12Hz in the motor cortex (blue). EEG and channel information (bottom). The overlap between the source activity one and two is around a 37.5% to 42% (marked in the gray area).

2.4.2 Relevance Analysis

We performed a relevance analysis based on the Q- α method, applying the Standard Power-Embedded Q- α algorithm. This method was originally proposed for feature selection in unsupervised and supervised inference problems (Wolf and Shashua, 2005; Wolf and Shashua, 2003), in which a set of features is weighted with an α vector coefficient according to the clustering quality of data points. Under this approach, let define the EEG data \mathbf{y} as the data points matrix with k samples, and each row correspond to an electrode containing the voltage information of a specific location as a feature to weight. Each electrode denoted

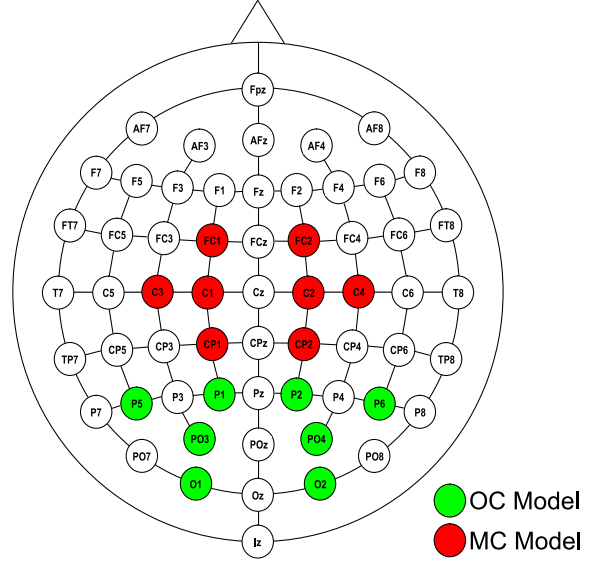


Figure 3: Electrode layout and selected local electrodes, local electrodes for OC partial brain model (green), and local electrodes for MC partial brain model (red).

by $\mathbf{y}_1^T, \dots, \mathbf{y}_k^T$ is pre-processed such that each electrode is centered around zero and its L_2 norm equal to one ($\|\mathbf{y}_i\| = 1$). Let define a vector $\alpha \in \mathbb{R}^d$, which contains the weight value associated with each electrode, being $\alpha = (\alpha_1, \dots, \alpha_d)^T$. Let \mathbf{A}_α be the corresponding affinity matrix defined as $\mathbf{A}_\alpha = \sum_{i=1}^d \alpha_i \mathbf{y}_i \mathbf{y}_i^T$ and $\mathbf{Q} \in \mathbb{R}^{k \times m}$ whose columns are the first m eigenvectors of \mathbf{A}_α associated with the highest eigenvalues $\lambda_1 \geq \dots \geq \lambda_m$. The values of α and \mathbf{Q} are unknown and they can be calculated solving the following optimization problem:

$$\begin{aligned} \max_{\mathbf{Q}, \alpha} \text{trace} \quad & (\mathbf{Q}^T \mathbf{A}_\alpha \mathbf{Q}) \\ \text{subject to} \quad & \alpha^T \alpha = 1, \mathbf{Q}^T \mathbf{Q} = \mathbf{I} \end{aligned} \quad (7)$$

by applying the Standard Power-Embedded Q- α algorithm to solve the optimization problem, the α weights are calculated. This method was applied before in a source reconstruction setting to weight the electrodes in an inverse problem solution algorithm presented by (Giraldo et al., 2012). In contrast, our proposed approach is to select a set of channels with the highest weights to perform the brain source reconstruction using the partial brain models. We defined three levels of relevance, based on the 4, 8 and 16 most relevant electrodes.

2.5 Brain Source Reconstruction

The source reconstruction is an estimation of the cortical activity using the registered voltages by elec-

trodes on the scalp. To estimate the neural activity in cortical regions, the EEG inverse problem must be solved. This problem is considered ill-posed and ill-conditioned due to the information available on the scalp, which is limited to hundreds of electrodes, while, the number of unknowns or sources to estimate is in the order of thousands.

Several methods provide a solution for the electromagnetic inverse problem based on electrodes information and the model of the conductivity. We selected two methods for brain mapping: the standardized low-resolution tomography sLORETA (Pascual-Marqui, 2002), and multiple sparse priors MSP (Friston et al., 2008). sLORETA was selected due to the low localization error presented by its author, even in some cases, zero error localization (Jatoi et al., 2014). On the other hand, MSP has been tested with low-density EEG montages by (Jatoi and Kamel, 2018) and has shown lower localization error than other methods like minimum norm estimation MNE and LORETA (López et al., 2014).

The MSP implementation used is a freely available software package SPM12 (Wellcome Trust Centre for Neuroimaging), we set up the number of patches to 1100 according to the findings using seven electrodes in (Jatoi and Kamel, 2018). The method sLORETA was implemented based on the code provided in by (Biscay et al., 2018).

2.6 Pipeline

The followed pipeline is summarized in Fig.4A. The procedure started with the simulation of the neural activity using Eq.6, two sources s_1 and s_2 were simulated. To generate the EEG signals, the activity matrix x is created and the sources were located in random positions, s_1 in occipital areas and s_2 in motor cortex areas, none of the sources was located outside the target to avoid a projection of an external source in the partial brain model. With the computed source activity x , and using the 10K model, the forward problem was calculated applying the Eq.1, the estimated EEG was contaminated with noise at five levels of signal-noise-ratio SNR of 0, 5, 10, 15, and 20dB. For detailed information of the EEG generation we refer to section 2.3.

Each EEG trial is filtered by using a high order FIR band-pass filters, the cutoff frequencies were set up at 19 and 21Hz for the first source s_1 , and for the second source s_2 were at 9 and 11Hz. The filters were applied in both direction of time to prevent losing information. As the output of the filter stage, two filtered set of EEG signals were obtained y_{s_1} and y_{s_2} for the respective simulated source.

After filtering, several EEG reductions were calculated according to the channel selection criteria, $y_{s_1_loe}$ and $y_{s_2_loe}$ by the local channel criterion, $y_{s_1_rel4e}$ and $y_{s_2_rel4e}$ by the first level of relevance with four electrodes, $y_{s_1_rel8e}$ and $y_{s_2_rel8e}$ by the second level of relevance with eight electrodes, and $y_{s_1_rel16e}$ and $y_{s_2_rel16e}$ by the third level of relevance with 16 electrodes.

The source reconstruction was performed with both methods MSP and sLORETA over all the ten EEG data, therefore, 20 source reconstructions were computed, four using the high-density montage with 60 electrodes and the 10K model, eight applying the channel selection criteria and the OC model, and eight applying the channel selection criteria and the MC model. A diagram with the name of each EEG data and the respective reconstructions is presented in Fig.4B.

Finally, the localization error was calculated comparing the resulting source position versus the original simulated position, using the following equation:

$$LocE = \|\hat{P}_x - P_x\|_2 \quad (8)$$

where P_x is the position in a 3D coordinated space of the simulated activity and \hat{P}_x the position of the maximum amplitude source of the estimated activity.

To provide a view of the effects of filtering, the same 20 reconstructions were calculated eliminating the filtering stage from the pipeline, making y_{s_1} and y_{s_2} equal to y , however, the same respective models were used to perform the source reconstruction stage. Because the source s_1 has higher mean power than s_2 due to the higher frequency, we were interested in evaluating the performance of the channel selection criteria and the brain mapping methods without isolating the sources using the filtering process.

3 RESULTS

A general view of the results is provided in Fig.5. At the top, the mean localization errors of the source reconstructions are presented, they were calculated eliminating the filtering stage from the pipeline. In contrast, at the bottom, the mean localization errors of the source reconstructions are presented using the complete pipeline. Additionally, the results are summarized in Table 1.

In a general point of view regarding the effects of filtering, when the filter stage was not applied (Fig. 5A and Table 1), the sources were mixed and the relevance criteria tended to select the channels related to the highest power source, in the case of the source s_1 ,

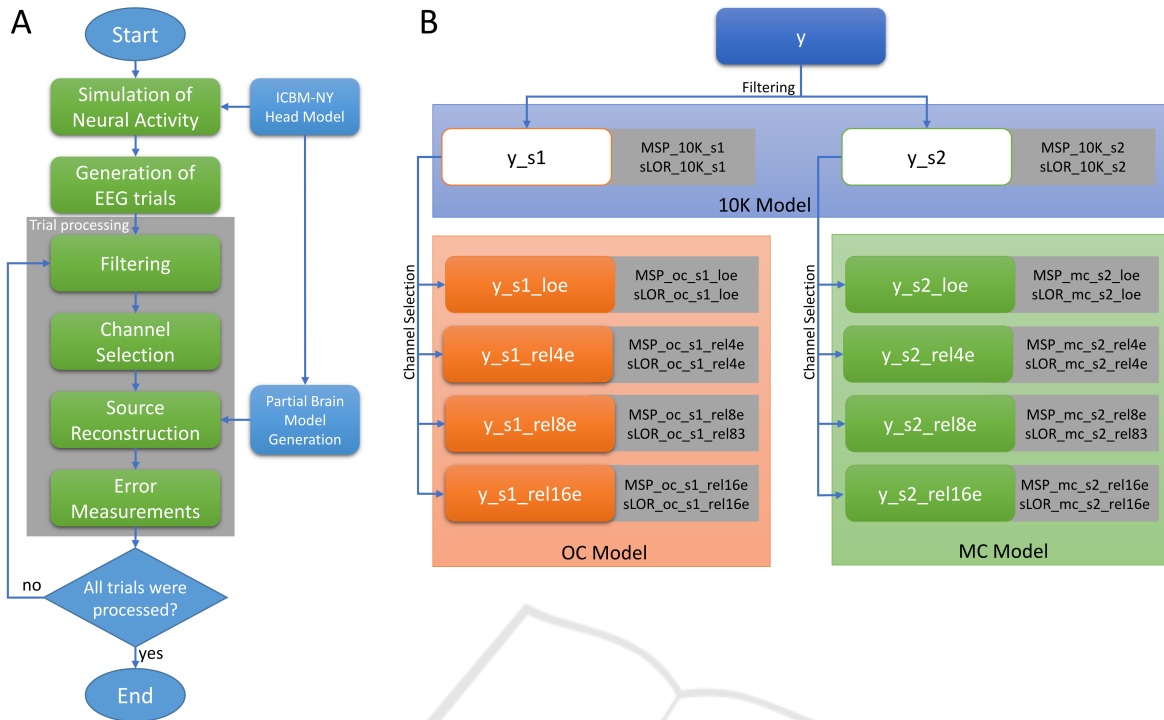


Figure 4: The flowchart of the followed pipeline (A), after the trial generation, the procedure is applied per trial (gray square). Source reconstruction tree (B), gray squares contain the name of the reconstruction using the EEG signal at left, the region in blue indicates the use of the 10K model, orange for the OC model, and green for the MC model.

due to the high frequency, it presents a higher power than source s_2 , therefore it was reconstructed with higher accuracy than s_2 . The accuracy obtained without filtering for the source s_2 shows that the methods projected the s_1 in the MC model, which explains the high mean localization error of the methods using the full set of electrodes. By inspection of the selected electrodes using the relevance criteria, in most of the cases, the electrodes were near to the source s_1 due to the lack of isolation by bypassing the filtering stage.

The best reconstructions were obtained by the full set of electrodes and the 10K model with filtering and without filtering for the sLORETA, in the case of MSP, the error increased significantly from 4 to 24 mm removing the filtering stage. Regarding the reconstructions using the presented pipeline and the partial brain models, the relevance channel selection with 16 electrodes obtained the lowest localization error for both sources, followed by the second level of relevance with 8 electrodes, the first level with 4 electrodes, and finally, the eight local electrodes. In all the cases the MSP method presented a low accuracy than sLORETA.

The local electrodes criteria presented a stable value for the reconstruction even if the filtering stage was not applied. For the source s_1 with OC model, the mean localization error was between 15 to 20 mm,

and for source s_2 and MC model, between 11 to 22 mm. In general, when used the partial brain models and the channel selection by relevance, the localization error remained below 10 mm for the sLORETA method, and below 21 mm for the MSP reconstructions.

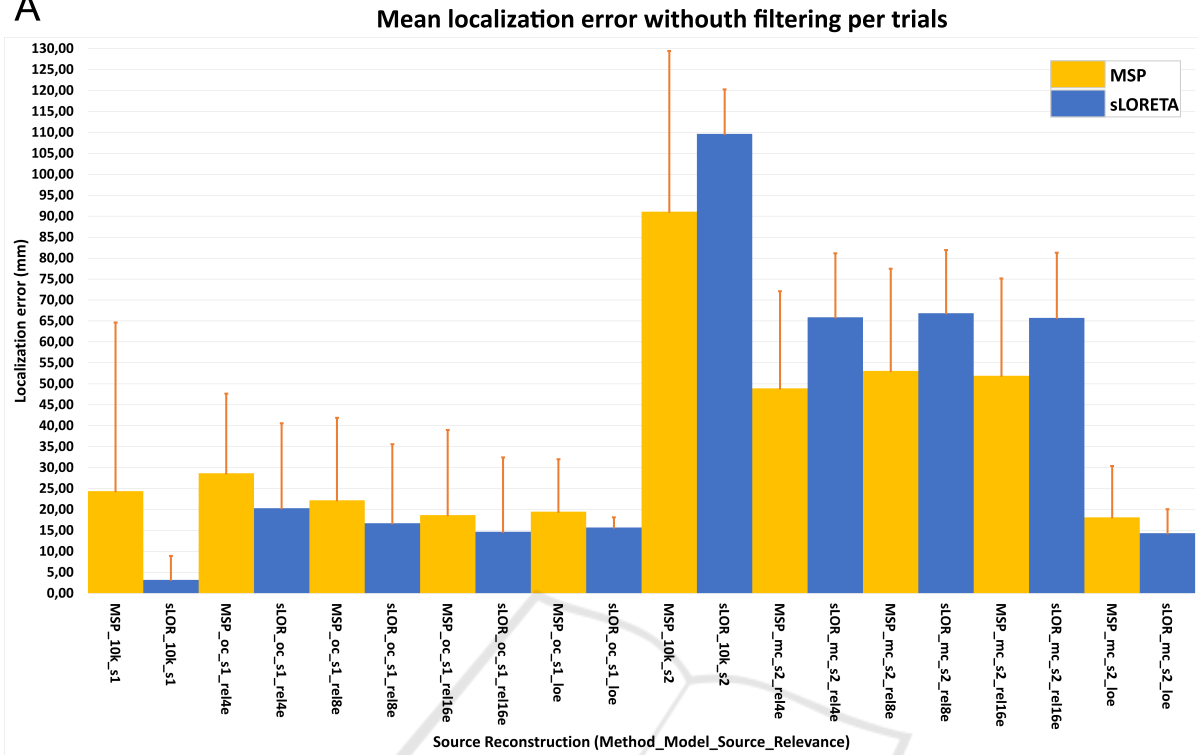
4 DISCUSSION

In this paper, we have presented a pipeline to reconstruct the source activity over specific brain regions using partial brain models and low-density EEG, using channel selection criteria.

In the presented simulations, we evaluated the performance of partial brain models and the relevance analysis for channel selection, the results showed by using of sLORETA the mean localization error were below 10mm, which in several cases is even low than localization error values obtained by other methods with high-density montages as explained in several works by (López et al., 2014; Jatoi and Kamel, 2018). Comparing to (López et al., 2014), we obtained a similar error value around 5 mm for our high-density montage with MSP.

The use of partial brain models constraint the

A



B

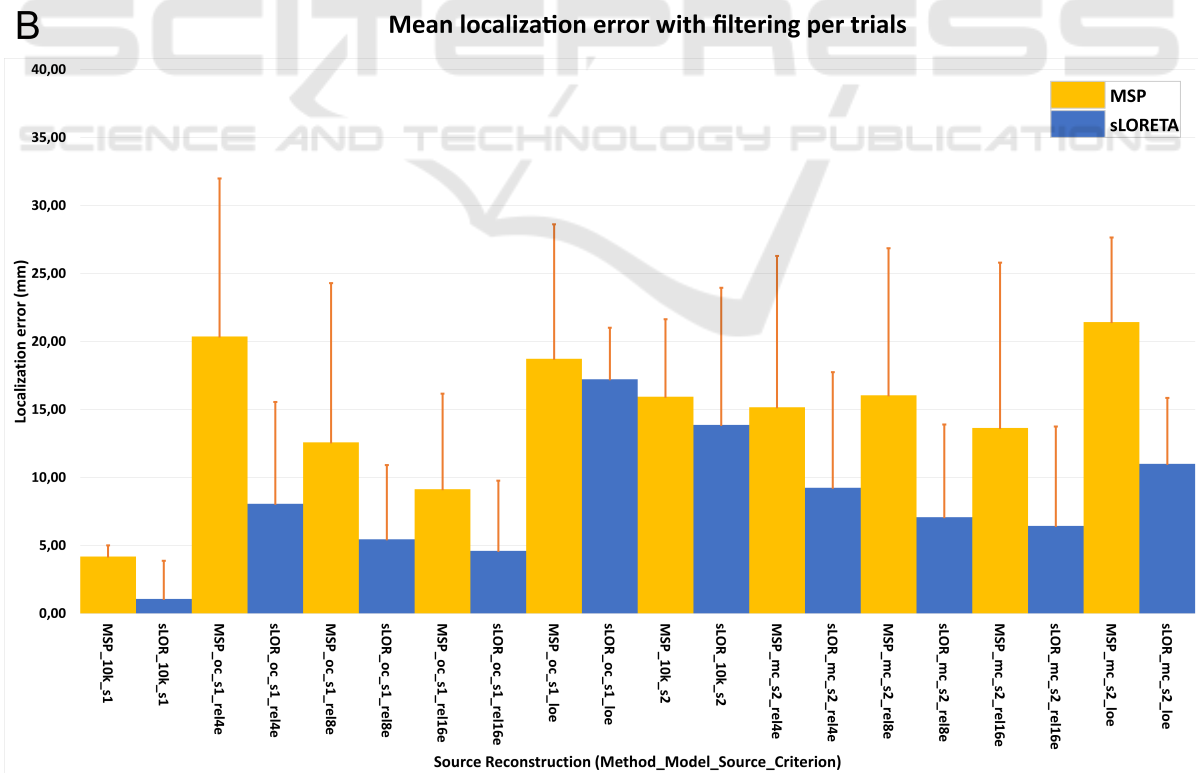


Figure 5: Mean error localization, without applying the filter stage (A), and following the complete pipeline with the filtering stage (B).

Table 1: Mean error localization without applying the filter stage, and following the complete pipeline including the filtering stage.

Method	Head Model	Source	Channel Selection Criteria	Number of Electrodes	Non-Filtered Data		Filtered Data	
					Mean Localization Error (mm)	SD	Mean Localization Error (mm)	SD
MSP	10K	S1	-	60	24,41	40,22	4,19	0,82
sLORETA	10K	S1	-	60	3,22	5,70	1,08	2,79
MSP	OC	S1	Relevance	4	28,67	18,97	20,37	11,63
sLORETA	OC	S1	Relevance	4	20,33	20,26	8,07	7,48
MSP	OC	S1	Relevance	8	22,19	19,69	12,58	11,72
sLORETA	OC	S1	Relevance	8	16,74	18,86	5,46	5,46
MSP	OC	S1	Relevance	16	18,68	20,29	9,14	7,02
sLORETA	OC	S1	Relevance	16	14,67	17,74	4,61	5,17
MSP	OC	S1	Local	8	19,47	12,54	18,73	9,89
sLORETA	OC	S1	Local	8	15,70	2,44	17,23	3,79
MSP	10K	S2	-	60	91,09	38,32	15,94	5,71
sLORETA	10K	S2	-	60	109,66	10,61	13,87	10,08
MSP	MC	S2	Relevance	4	48,90	23,16	15,17	11,13
sLORETA	MC	S2	Relevance	4	65,88	15,25	9,24	8,51
MSP	MC	S2	Relevance	8	53,09	24,39	16,05	10,82
sLORETA	MC	S2	Relevance	8	66,83	15,07	7,09	6,82
MSP	MC	S2	Relevance	16	51,93	23,19	13,64	12,17
sLORETA	MC	S2	Relevance	16	65,71	15,61	6,44	7,30
MSP	MC	S2	Local	8	18,14	12,27	21,44	6,22
sLORETA	MC	S2	Local	8	14,34	5,71	11,01	4,85

brain mapping methods to find a solution in a pre-defined space, which will make it prone to error when the source of interest originates from other areas. For this reason, the application of partial brain models should be restricted to applications in which the area of interest that will be activated is well known, i.e., in some visual evoked potentials VEP experiments in which the interest is to know how the visual cortex areas respond to certain stimuli (Vilhelmsen et al., 2019; Van Der Meer et al., 2013), or in motor imaginary task where it is well known that the motor cortex is activated (Burianová et al., 2013; Qiu et al., 2017).

Even if the results shown that the localization error was higher with the local electrodes than applying the relevance criteria, this method can be applied in settings in which a high quantity of electrodes is not available. In addition, we consider that the use of local electrodes can be applied in settings for which the frequency of the source of interest is not well known. As shown in Fig.5 and Table 1, the mean error was kept below 22 mm regardless of the use of filters to isolate the sources.

It is clear, regardless of the use of the filtering stage, that the best reconstructions were obtained by the full set of electrodes. However, it is noticeable that with the presented pipeline using low-density EEG

montages and the proposed partial brain models, we achieved with eight electrodes a mean localization error around 7 mm with sLORETA and 16 mm with MSP, and slightly less with 16 electrodes, around 6 mm with sLORETA and 14 mm with MSP.

5 CONCLUSIONS

In this work, we presented a formal definition of the partial brain models and tested the capability to mapping a target zone of the brain using a reduced model of a region of interest. We presented a pipeline to apply those models and performed experiments with multiple synthetic EEG trials with two overlapped sources at several levels of noise and several levels of electrode resolution based on channel selection criteria. We measured the quality of the source reconstructions with the localization error, and based on the accuracy of the results obtained herein, we consider that partial brain models following the pipeline can reconstruct the source activity using low-density EEG montages of 8 and 16 electrodes with a precision below 10 mm with sLORETA and 20 mm with MSP.

As presented, we focused on the localization error obtained with sLORETA and MSP for brain source

reconstruction, however, it is worth noticing that the solutions by sLORETA are smooth (Pascual-Marqui, 2002), while the other hand, MSP present more sparse solutions (López et al., 2014; Friston et al., 2008). Therefore in future works, we will consider the use of error measurements that involve the temporal evolution of the reconstructed sources and the sparseness of the solutions.

The pipeline presented considers a basic filter stage using band-pass filters with the intention to focus on the partial brain models to source activity reconstruction. However, several studies (Muñoz-Gutiérrez et al., 2018; Hansen et al., 2019) have shown that the using of advanced techniques for frequency decomposition like empirical mode decomposition EMD, multivariate EMD, noise assisted EMD, and wavelets can offer a solution for unmixing the source activity improving the brain mapping algorithms. Those techniques will be studied on partial brain models in future publications.

AUTHOR CONTRIBUTIONS

This part was intentionally removed for reviewing purposes All the authors conceived and designed the experiments. AFS performed the experiments. All the authors analyzed the data, wrote and refined the article.

ACKNOWLEDGMENT

This part was intentionally removed for reviewing purposes This work was supported by the Norwegian University of Science and Technology NTNU, project "David and Goliath: single-channel EEG unravels its power through adaptive signal analysis".

REFERENCES

- Biscay, R. J., Bosch-Bayard, J. F., and Pascual-Marqui, R. D. (2018). Unmixing EEG Inverse solutions based on brain segmentation. *Frontiers in Neuroscience*, 12(MAY).
- Burianová, H., Marstaller, L., Sowman, P., Tesan, G., Rich, A. N., Williams, M., Savage, G., and Johnson, B. W. (2013). Multimodal functional imaging of motor imagery using a novel paradigm. *NeuroImage*.
- Fonov, V., Evans, A., McKinstry, R., Almlí, C., and Collins, D. (2009). Unbiased nonlinear average age-appropriate brain templates from birth to adulthood. *NeuroImage*, 47:S102.
- Friston, K., Harrison, L., Daunizeau, J., Kiebel, S., Phillips, C., Trujillo-Barreto, N., Henson, R., Flandin, G., and Mattout, J. (2008). Multiple sparse priors for the M/EEG inverse problem. *NeuroImage*, 39(3):1104–1120.
- Giraldo, E., Peluffo-Ordoñez, D., and Castellanos-Dominguez, G. (2012). Weighted Time Series Analysis for Electroencephalographic Source Localization. *DYNA Universidad Nacional de Colombia*, 79:64–70.
- Hämäläinen, M. S. and Ilmoniemi, R. J. (1994). Interpreting magnetic fields of the brain: minimum norm estimates. *Medical & Biological Engineering & Computing*, 32(1):35–42.
- Hansen, S. T., Hemakom, A., Gylling Safeldt, M., Krohne, L. K., Madsen, K. H., Siebner, H. R., Mandic, D. P., and Hansen, L. K. (2019). Unmixing oscillatory brain activity by EEG source localization and empirical mode decomposition. *Computational Intelligence and Neuroscience*, 2019.
- Huang, Y., Parra, L. C., and Haufe, S. (2016). The new york head—a precise standardized volume conductor model for eeg source localization and tes targeting. *NeuroImage*, 140:150–162. Transcranial electric stimulation (tES) and Neuroimaging.
- Jatoi, M. A. and Kamel, N. (2018). Brain source localization using reduced eeg sensors. *Signal, Image and Video Processing*, 12(8):1447–1454.
- Jatoi, M. A., Kamel, N., Malik, A. S., Faye, I., and Begum, T. (2014). A survey of methods used for source localization using eeg signals. *Biomedical Signal Processing and Control*, 11:42–52.
- López, J. D., Litvak, V., Espinosa, J. J., Friston, K., and Barnes, G. R. (2014). Algorithmic procedures for Bayesian MEG/EEG source reconstruction in SPM. *NeuroImage*, 84:476–487.
- Muñoz-Gutiérrez, P. A., Giraldo, E., Bueno-López, M., and Molinas, M. (2018). Localization of active brain sources from EEG signals using empirical mode decomposition: a comparative study. *Frontiers in Integrative Neuroscience*, 12.
- O’Leary, J. (1970). Hans berger on the electroencephalogram of man. the fourteen original reports on the human electroencephalogram. translated from the german and edited by pierre floor. *Science*, 168:562–563.
- Pascual-Marqui, R. D. (2002). Standardized low-resolution brain electromagnetic tomography (sLORETA): Technical details. *Methods and Findings in Experimental and Clinical Pharmacology*, 24(SUPPL. D):5–12.
- Pascual-Marqui, R. D., Michel, C., and Lehmann, D. (1994). Low resolution electromagnetic tomography: a new method for localizing electrical activity in the brain. *International Journal of Psychophysiology*, 18(1):49–65.
- Qiu, Z., Allison, B. Z., Jin, J., Zhang, Y., Wang, X., Li, W., and Cichocki, A. (2017). Optimized motor imagery paradigm based on imagining Chinese characters writing movement. *IEEE Transactions on Neural Systems and Rehabilitation Engineering*, 25(7):1009–1017.
- Soler, A., Giraldo, E., and Molinas, M. (2019). Partial Brain Model For Real-Time Classification Of RGB Visual

- Stimuli: A Brain Mapping Approach To BCI. In *8th Graz Brain Computer Interface Conference*.
- Van Der Meer, A. L., Svantesson, M., and Van Der Weel, F. R. (2013). Longitudinal study of looming in infants with high-density EEG. *Developmental Neuroscience*, 34(6):488–501.
- Vilhelmsen, K., Agyei, S. B., van der Weel, F. R., and van der Meer, A. L. (2019). A high-density EEG study of differentiation between two speeds and directions of simulated optic flow in adults and infants. *Psychophysiology*, 56(1).
- Vorwerk, J., Clerc, M., Burger, M., and Wolters, C. H. (2012). Comparison of boundary element and finite element approaches to the EEG forward problem. *Biomedizinische Technik*, 57:795–798.
- Wolf, L. and Shashua, A. (2003). Feature selection for unsupervised and supervised inference: The emergence of sparsity in a weighted-based approach. In *Proceedings of the IEEE International Conference on Computer Vision*, volume 1, pages 378–384.
- Wolf, L. and Shashua, A. (2005). Feature Selection for Unsupervised and Supervised Inference: The Emergence of Sparsity in a Weight-Based Approach * Amnon Shashua. *Journal of Machine Learning Research*, 6:1855–1887.

